Applied Physics Letters ARTICLE scitation.org/journal/apl

High-frequency and below bandgap anisotropic dielectric constants in α-$(Al_xGa_{1-x})_2O_3$ $(0 \le x \le 1)$

Cite as: Appl. Phys. Lett. **119**, 092103 (2021); doi: 10.1063/5.0064528
Submitted: 23 July 2021 · Accepted: 17 August 2021 ·
Published Online: 2 September 2021

View Online Export Citation CrossMark

Matthew Hilfiker,[1,a)] Ufuk Kilic,[1] Megan Stokey,[1] Riena Jinno,[2,3] Yongjin Cho,[2] Huili Grace Xing,[2,4] Debdeep Jena,[2,4] Rafał Korlacki,[1] and Mathias Schubert[1,5,6]

AFFILIATIONS

[1]Department of Electrical and Computer Engineering, University of Nebraska-Lincoln, Lincoln, Nebraska 68588, USA
[2]School of Electrical and Computer Engineering, Cornell University, Ithaca, New York 14853, USA
[3]Department of Electronic Science and Engineering, Kyoto University, Kyoto 615-8510, Japan
[4]Department of Material Science and Engineering, Cornell University, Ithaca, New York 14853, USA
[5]Terahertz Materials Analysis Center and Center for III-N technology, C3NiT – Janzèn, Department of Physics, Chemistry and Biology (IFM), Linköping University, 58183 Linköping, Sweden
[6]Leibniz Institut für Polymerforschung e.V., 01069 Dresden, Germany

[a)]**Author to whom correspondence should be addressed:** mhilfiker2@unl.edu. **URL:** http://ellipsometry.unl.edu

ABSTRACT

A Mueller matrix spectroscopic ellipsometry approach was used to investigate the anisotropic dielectric constants of corundum α-$(Al_xGa_{1-x})_2O_3$ thin films in their below bandgap spectral regions. The sample set was epitaxially grown using plasma-assisted molecular beam epitaxy on *m*-plane sapphire. The spectroscopic ellipsometry measurements were performed at multiple azimuthal angles to resolve the uniaxial dielectric properties. A Cauchy dispersion model was applied, and high-frequency dielectric constants are determined for polarization perpendicular ($\varepsilon_{\infty,\perp}$) and parallel ($\varepsilon_{\infty,\parallel}$) to the thin film *c*-axis. The optical birefringence is negative throughout the composition range, and the overall index of refraction substantially decreases upon incorporation of Al. We find small bowing parameters of the high-frequency dielectric constants with $b_\perp = 0.386$ and $b_\parallel = 0.307$.

The ultra-wide bandgap material Ga_2O_3 has gained significant attention as a potential material for next-generation high power electronics. Within the last decade, of the five polymorphs (α, β, γ, δ, and ϵ),[1] the thermodynamically stable monoclinic phase (β-Ga_2O_3) has received growing attention with the availability of large-scale single-crystal substrates with low-defect densities.[2]

The metastable corundum phase (α-Ga_2O_3) has gained recent interest because of its higher symmetry (uniaxial) and slightly larger bandgap.[3] A major advantage of the Ga_2O_3 polymorphs over conventional wide bandgap semiconductors, such as SiC or GaN, is a large estimated Baliga figure of merit (e.g., ≈3200 for β-Ga_2O_3). This results from its substantial critical field and intrinsic mobility, which leads to potential for considerable improvement over GaN (846) and 4H-SiC (317) in performance of electronic power devices.[2,4] α-Ga_2O_3-based devices could further benefit from an even higher critical field than β-Ga_2O_3 due to its larger bandgap energy.[3] Thus, an even larger Baliga figure of merit is anticipated, assuming that charge transport mechanisms are similar to those in β-Ga_2O_3. Furthermore, it has been proven that α-Ga_2O_3 as well as aluminum alloys, α-$(Al_xGa_{1-x})_2O_3$, can be deposited at lower temperatures on sapphire substrates, providing the capability for a more cost-effective fabrication process.[5,6]

Through alloying with a similarly structured material, one can modify and greatly change the material properties, such as bandgap energy and index of refraction. A recent example is the system $Al_xGa_{1-x}N$, which is used for creation of devices, such as high-electron mobility transistors,[7] laser diodes,[8,9] and solar-blind photodetectors.[10] Exact knowledge of bandgap energy and refractive index dependencies on composition, for example, permits creation of multiple layer $Al_xGa_{1-x}N$ Bragg reflectors through varying the Al content in each layer.[11,12] The ultra-wide bandgap system $(Al_xGa_{1-x})_2O_3$ unlocks the deep ultraviolet spectral region through its much larger bandgap energies than $Al_xGa_{1-x}N$.[13] Density functional theory (DFT) calculations predict tunability of the bandgap in $(Al_xGa_{1-x})_2O_3$ for both the α and β phases,[13,14] between Ga_2O_3 (4.9 eV)[15–18] and Al_2O_3 (8.8 eV).[19] Of fundamental importance for design of future electronic and optoelectronic devices is the accurate knowledge of the

below-bandgap spectral region index of refraction as a function of photon energy and alloy composition. In addition, for the optically uniaxial α-phase, which possesses corundum structure, information about the anisotropy, i.e., the difference between the ordinary (polarization perpendicular to the lattice c axis; ⊥) and extraordinary (parallel to c; ||) is required. The below-bandgap index of refraction at photon energies much less than the bandgap energy, $\hbar\omega \ll E_g$, directly relates to the so-called high-frequency dielectric constant, $n_{\hbar\omega \ll E_g} \approx \sqrt{\varepsilon_\infty}$, which is also related to the static dielectric constant at $\hbar\omega \approx 0$, ε_{DC}, through the knowledge of the optical phonon modes and the Lyddane–Sachs–Teller relation.[20] We note that complete sets of optical phonon modes are not known presently for α-$(Al_xGa_{1-x})_2O_3$.

For β-$(Al_xGa_{1-x})_2O_3$, research on growth has been reported with phase diagrams predicting the possibility of $x \leq 0.7$ content crystals.[1] Single crystal growth of the β-phase using plasma assisted molecular beam epitaxy (PAMBE) is currently limited to contents of $x \leq 0.21$ due to growth temperature constraints.[21,22] The α-phase does not have this constraint as it does not require the same high-temperature fabrication process as the β-phase.[23] Additionally, α-Ga_2O_3 and α-Al_2O_3 both exhibit the same corundum crystal structure, while β-Al_2O_3 is not known as a possible stable compound under normal conditions. Multiple methods have been proposed for fabrication of α-$(Al_xGa_{1-x})_2O_3$ including solvothermal synthesis,[24] mist chemical vapor deposition (mist-CVD),[25–29] plasma assisted pulsed laser deposition (PLD),[30] and molecular beam epitaxy (MBE).[23,31] A difficulty with depositing the α-phase is its natural tendency to form β-phase. Recently, Jinno *et al.* found that epitaxial growth on *m*-plane sapphire can suppress beta-phase formation, leading to pure-phase single-crystal α-$(Al_xGa_{1-x})_2O_3$ growth.[23]

Only few optical investigations are known for α-$(Al_xGa_{1-x})_2O_3$. Ito *et al.* determined bandgap parameters for mist-CVD deposited thin films using unpolarized optical transmission spectra.[25] Dang *et al.* used transmittance data to estimate bandgap values using multiple model analysis methods, including Tauc, Tauc–Lorentz, and O'Leary–Johnson–Lim models.[28] Using photoelectron spectroscopy, Chen *et al.*[30] and Uchida *et al.*[27] estimated bandgap parameters in PLD grown and mist-CVD grown thin films, respectively. Jinno *et al.* determined bandgap values from transmission measurements for PAMBE grown thin films on *m*-plane sapphire.[23] Anisotropic refractive indices and polarization dependent band-to-band transitions and exciton properties were reported for α-Ga_2O_3 by Kracht *et al.*[32] and Hilfiker *et al.*[3] using spectroscopic ellipsometry. No information is available for the below-bandgap index of refraction, anisotropy, and polarization dependencies of the bandgap energies for α-$(Al_xGa_{1-x})_2O_3$ with $x > 0$.

Generalized spectroscopic ellipsometry (GSE) is an accurate measurement technique for determining the anisotropic dielectric functions of materials.[33] GSE has been extensively used to investigate high-frequency dielectric properties in ultra-wide bandgap metal oxide materials, such as $ZnGa_2O_4$,[34] β-Ga_2O_3,[15–17] α-Ga_2O_3,[3,32] and β-$(Al_xGa_{1-x})_2O_3$.[22] Limited knowledge exists on the high-frequency dielectric constants of α-Ga_2O_3. Spectroscopic ellipsometry was performed on *r*-plane oriented α-Ga_2O_3 thin films fabricated using PAMBE by Kracht *et al.* Anisotropic high-frequency dielectric constants of $\varepsilon_{\infty,\perp} = 3.75$ and $\varepsilon_{\infty,||} = 3.64$ were found.[32] Hilfiker *et al.* used GSE on *m*-plane thin films and obtained $\varepsilon_{\infty,\perp} = 3.86$ and $\varepsilon_{\infty,||} = 3.76$.[3] In this present study, we use GSE and analyze a set of PAMBE grown single-crystal α-$(Al_xGa_{1-x})_2O_3$ thin films for $0 \leq x \leq 1$. We apply a Cauchy dispersion analysis and determine the below-bandgap high-frequency dielectric properties, including anisotropy.

PAMBE was used to fabricate α-$(Al_xGa_{1-x})_2O_3$ thin films on *m*-plane sapphire spanning the entire Al content range, including thin films of α-Ga_2O_3 and α-Al_2O_3. Oxygen plasma treatment was applied to each sapphire substrate prior to growth. All samples were grown using a radio frequency plasma source ($RF_{power} = 250$ W) and an oxygen flow rate of 0.50 sccm. Substrate temperatures were 650 °C and 750 °C for compositions $x < 1$ and $x = 1$, respectively. Asymmetrical reciprocal space maps indicate fully lattice relaxed α-$(Al_xGa_{1-x})_2O_3$ films for $x < 0.37$ and films with $(0.37 \leq x \leq 0.74)$ consist of coherent and relaxed layers, and the relaxed layers are subject to slight in-plane compressive strain.[23] Note that both α-Ga_2O_3 and α-Al_2O_3 thin films are completely unstrained. The thin films adopt the same *m*-plane orientation than the substrate. Additional growth details and structural analysis are reported by Jinno *et al.*[23] We note the samples with $x = 0$ and $x = 0.18$ are grown under similar conditions but different from those shown in Ref. 23.

Room temperature GSE data in Mueller matrix format were acquired. A dual-rotating compensator ellipsometer (RC2, J. A. Woollam Co., Inc.) measured data across the spectral range of 0.73 to 6.42 eV. Measurements were performed for three angles of incidence ($\Phi_a = 50°, 60°, 70°$) and in 15° azimuthal rotation steps for a complete rotation. Selected experimental Muller matrix data are shown in Fig. 1, for the 18% Al content film.

The α-$(Al_xGa_{1-x})_2O_3$ thin films are optically uniaxial with the *c*-plane perpendicular to the sample normal. Therefore, both ordinary ($\varepsilon_\perp$) and extraordinary dielectric functions ($\varepsilon_{||}$) can be assessed within the sample surface. For our GSE analysis, we employ the dielectric function tensor

$$\varepsilon = \begin{pmatrix} \varepsilon_\perp & 0 & 0 \\ 0 & \varepsilon_\perp & 0 \\ 0 & 0 & \varepsilon_{||} \end{pmatrix}. \quad (1)$$

Euler angle definitions are applied during the analysis of GSE data acquired at multiple sample azimuth rotations to define the proper dielectric tensor orientation with respect to sample placement in the ellipsometer setup.[35] For the below-bandgap spectral range, it is assumed that the extinction coefficient (k) is zero for all photon energies $\hbar\omega$. A Cauchy dispersion equation can be applied to render the spectral behavior of the refractive index

$$n_j(\lambda) = A_j + \frac{B_j}{\lambda^2} + \frac{C_j}{\lambda^4} + \cdots, \quad j = \text{“}\perp\text{”}, \text{“}||\text{”}, \quad (2)$$

where A_j, B_j, and C_j are the Cauchy model parameters, $\lambda = \frac{2\pi c}{\omega}$ is the light wavelength, and c is the speed of light. Note that $\varepsilon_{\infty,j} = A_j^2$. A substrate-film-overlayer model approach is applied to model the Mueller matrix data. The overlayer is implemented to account for surface effects. We define this layer as an effective medium containing 50% void ($\varepsilon_r = 1$) and 50% the isotropic average of the underlying film optical constants. Both the surface overlayer and α-$(Al_xGa_{1-x})_2O_3$ layers have an associated film thickness denoted as t_{ov} and t_{AlGO}, respectively. The optical constants for the sapphire substrate were obtained using the same Cauchy approach and measured data from a single-crystalline *m*-plane sapphire substrate. These values for sapphire were fixed for the remainder of the analysis.

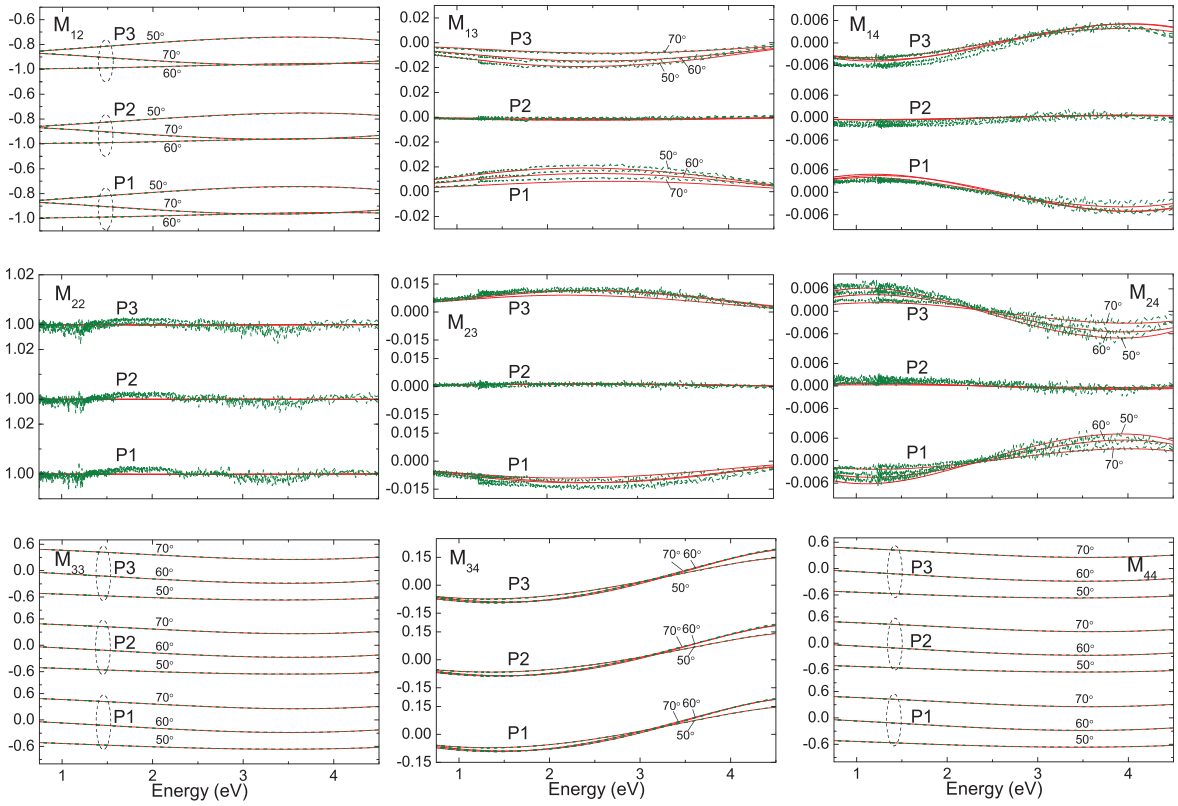

FIG. 1. Best match model (solid, red lines) and experimental (dotted, green lines) Mueller matrix spectroscopic ellipsometry data. Data were measured from PAMBE grown single-crystal α-$(Al_{0.18}Ga_{0.82})_2O_3$ on an *m*-plane sapphire substrate. Data were acquired at three angles of incidence ($\Phi_a = 50°$, 60°, 70°) with select azimuthal rotations [P1: $\varphi = 48.(7)°$, P2: $\varphi = 93.(7)°$, P3: $\varphi = 138.(7)°$] shown. Euler angle parameters consistent with the uniaxial orientation $\theta = 90°$ and $\psi = 0°$ were fixed for the analysis. The anisotropy is reflected in the non-vanishing off block Mueller matrix elements $M_{13,31}$, $M_{14,41}$, $M_{23,32}$, and $M_{24,42}$, and changes in all elements upon rotation. Note that elements with equivalent indices, e.g., $M_{13,31}$, are equal, and only one of each pair is shown.

The best match model calculated Muller matrix data are shown compared with the experimental data in Fig. 1, for the 18% Al content film. Other Al content measured data are shown in the supplementary material. We see an excellent agreement between the model calculated data and the experimental data across the entire sample set. For higher concentrations of Al, M_{14} approaches the uncertainty limit of the ellipsometry measurement. However, information regarding the birefringence of the sample is still captured in the other matrix elements. Note that small discontinuities found around 1.2–1.3 eV are caused by subtle calibration parameter uncertainties associated with the transition between two different detector arrays in our instrument in this spectral range. Model parameters film thickness and surface roughness are given in Table I. The structural parameters for the sample set, film thickness, and surface roughness were previously investigated by Jinno *et al.* using a combination of x-ray reflectivity (XRR) and atomic force microscopy (AFM).[23] Note that for the sample with $x = 1$, the XRR thickness parameter was assumed for GSE analysis. Deviations in surface roughness values obtained from AFM and GSE analysis can be attributed to AFM using a root mean square calculation compared to ellipsometry, which determines an effective surface roughness layer thickness, and GSE averaging over an area approximately 6–7 orders of magnitude larger than the AFM measurements. This has been shown in further detail by Petrik *et al.* where they performed a comparative analysis between AFM and spectroscopic ellipsometry (SE) of surface roughness for polysilicon films.[36] With the differing roughness methodology accounted for, we note quite reasonable agreement between the α-$(Al_xGa_{1-x})_2O_3$ thin film thickness parameters obtained here and by Jinno *et al.*[23]

The resulting best match dielectric functions as determined from the Cauchy dispersion equation are shown in Fig. 2, for all compositions investigated here, and with data for the sapphire substrate for comparison. The list of Cauchy parameters is given in Table I. Higher order terms were disregarded, as they had no discernible effect on the best match model calculations. We note excellent agreement for results with $x = 0$ between data reported here and our previous work.[3] The *m*-plane sapphire substrate results ($\varepsilon_{\infty,\perp} = 3.063$ and $\varepsilon_{\infty,\parallel} = 3.036$) are in excellent agreement with those determined by Harman *et al.* ($\varepsilon_{\infty,\perp} = 3.064$ and $\varepsilon_{\infty,\parallel} = 3.038$).[19,37] The thin film results for $x = 1$ are in perfect agreement with our substrate data within the error margins. The dielectric constants substantially decrease with the increasing Al content. This can be understood by the fact that Al (13) has a smaller atomic number than Ga (32) and, which may result in a smaller overall polarizability, hence, smaller index of refraction. It is also noted that the difference between ordinary and extraordinary

TABLE I. Cauchy dispersion parameters for α-$(Al_xGa_{1-x})_2O_3$ as a function of Al alloy composition. Structural parameters are compared to those presented for the same sample set reported in Ref. 23. Refer to Eq. (2) for parameter definitions. Note that parameter A is directly related to the high-frequency dielectric function ($\varepsilon_\infty = A^2$). The last digit is determined with 90% confidence, which is indicated with parentheses for each parameter.

Jinno *et al.*[23]			This work[a]					
Al Content[b] (%)	t_{AlGO}[c] (nm)	t_{ov}[d] (nm)	t_{AlGO} (nm)	t_{ov} (nm)	$A_\perp$ (-)	$B_\perp$ (μm^2)	$A_\parallel$ (-)	$B_\parallel$ (μm^2)
0	51.8	0.96	48.0(8)	3.6(3)	1.965(8)	0.0129(4)	1.938(2)	0.0132(8)
18	56.7	0.95	53.1(7)	3.4(0)	1.920(3)	0.0117(1)	1.898(3)	0.0118(2)
37	66	0.78	63.0(2)	4.2(2)	1.865(1)	0.0099(0)	1.848(4)	0.0100(3)
54	84.3	0.97	79.7(2)	2.3(2)	1.825(2)	0.0080(5)	1.815(1)	0.0084(1)
59	63.8	3.5	62.0(8)	5.1(8)	1.805(9)	0.0077(8)	1.793(5)	0.0081(1)
100	40	0.52	40	7.1(4)	1.747(5)	0.0062(9)	1.739(5)	0.0061(9)
substrate	...	...	...	3.8(6)	1.750(0)	0.0059(7)	1.742(4)	0.0058(3)

[a]From Cauchy dispersion model as described above.
[b]Determined from x-ray diffraction (XRD) and x-ray photoelectron spectroscopy (XPS).
[c]Determined from x-ray reflectometry (XRR) measurements.
[d]Root mean square surface roughness from atomic force microscopy (AFM) for a 2×2 μm^2 square size.

dielectric constants (indices of refraction) reduces with the increasing Al content, reaching smallest birefringence for sapphire, the binary end point. Additionally, the birefringence is shown to decrease with an increase in photon energies, which is reflected by the B-terms in the Cauchy dispersion equations being smaller for the ordinary direction than for the extraordinary direction.

Figure 3 shows $\varepsilon_{\infty,\perp}$ and $\varepsilon_{\infty,\parallel}$ from the best match Cauchy model. We observe a non-linear dependence on Al content and define a bowing parameter, b_j,

$$\varepsilon_{\infty,j}[x] = (1-x)\varepsilon_{\infty,j}[0] + x\varepsilon_{\infty,j}[1] - b_j x(1-x). \quad (3)$$

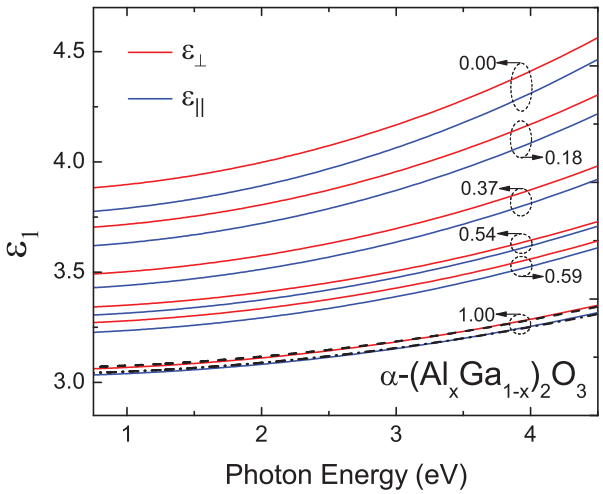

FIG. 2. $\varepsilon_{1,\perp}$ (red solid lines) and $\varepsilon_{1,\parallel}$ (blue solid lines) for α-$(Al_xGa_{1-x})_2O_3$ as determined from the Cauchy dispersion equation. Black dashed and dash dot lines represent $\varepsilon_{1,\perp}$ and $\varepsilon_{1,\parallel}$ for the m-plane sapphire substrate, respectively. Note that lines and symbols for $x = 1$ are nearly indistinguishable between substrate and thin film results because the data are near virtually identical.

We find a larger associated bowing parameter with the ordinary direction ($b_\perp = 0.386$) compared to the extraordinary ($b_\parallel = 0.307$). Bowing parameters associated with the bandgap shift due to an increase in aluminum content has been the subject of both theoretical[13,14] and experimental studies.[23] Each study determined a positive isotropic bowing parameter, while disregarding the uniaxial anisotropy. This is in agreement with the positive bowing parameters determined from this study and matches expectations of a positive bowing parameter from the large bandgap mismatch of Ga_2O_3 and Al_2O_3 and associated compositional disorder.

Mismatch in the lattice spacing between the α-$(Al_xGa_{1-x})_2O_3$ thin films and Al_2O_3 substrate potentially induces tensile strain. While both binary thin films for $x = 0$ and $x = 1$ are fully strain free, the former because of complete lattice relaxation and the latter because of

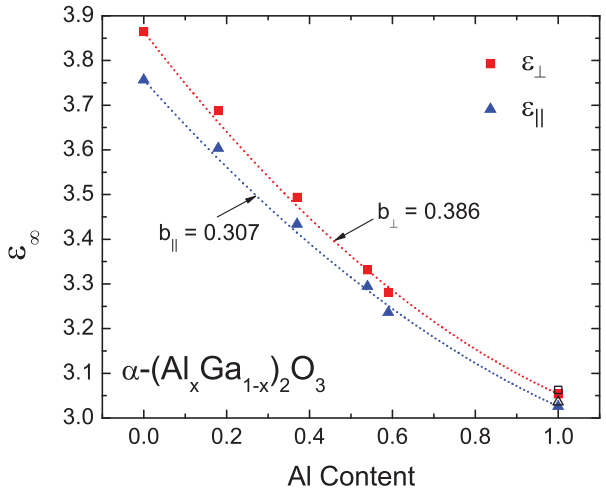

FIG. 3. $\varepsilon_{\infty,\perp}$ (red squares) and $\varepsilon_{\infty,\parallel}$ (blue triangles) for α-$(Al_xGa_{1-x})_2O_3$ as determined from the Cauchy dispersion extrapolation. Short dashed lines indicate the best fit to Eq. (3) with associated bowing parameter b. Black square and triangle indicate $\varepsilon_{\infty,\perp}$ and $\varepsilon_{\infty,\parallel}$ for the m-plane sapphire substrate, respectively.

complete lattice match, the epitaxial films for $0.37 \leq x \leq 0.74$ consist of partially or fully relaxed content only, and strain induced effects cannot be ruled out.[23] Thus, it may be possible that some contribution to the bowing parameters originate from finite strain effects. It is well known that strain and stress affect the optical properties of thin films, and further detailed investigations will be necessary. However, the linear stress coefficients for the ordinary and extraordinary indices of refraction were reported for GaN, which would require hundreds of MPa stress in order to produce significant contributions here, i.e., outside of the uncertainty limits, assuming similar order of stress coefficients for α-Ga_2O_3 than GaN.[38] Likewise, further quantitative studies are required for identifying the strain–stress relationships for the refractive indices in α-Ga_2O_3. We, therefore, ignore the anisotropic strain effects due to their expected small contributions within the uncertainty range of our analysis.

In summary, we have determined the anisotropic optical constants in the below bandgap spectral region, including the high-frequency dielectric constants for a set of α-$(Al_xGa_{1-x})_2O_3$ single-crystal thin films grown using PAMBE. The dielectric functions were determined using a Cauchy dispersion equation to describe the Mueller matrix spectroscopic ellipsometry measured data across the spectral range of 0.75 to 4.5 eV. We find that the Cauchy model-based results are in excellent agreement with the experimental data. All compositions exhibit uniaxial negative birefringence across the measured spectral range. A slightly larger bowing parameter is observed for the ordinary direction. Overall, the index of refraction substantially decreases with the incorporation of Al.

See the supplementary material for experimental and best match model-based Mueller matrix data for all samples investigated in this work.

This work was supported in part by the National Science Foundation (NSF) under Award Nos. NSF DMR 1808715 and NSF/EPSCoR RII Track-1: Emergent Quantum Materials and Technologies (EQUATE), Award No. OIA-2044049; by Air Force Office of Scientific Research under Award Nos. FA9550-18-1-0360, FA9550-19-S-0003, and FA9550-21-1-0259; by ACCESS, an AFOSR Center of Excellence, under Award No. FA9550-18-1-0529; and by the Knut and Alice Wallenbergs Foundation award "Wide-bandgap semiconductors for next generation quantum components." M. S. acknowledges the University of Nebraska Foundation and the J. A. Woollam Foundation for financial support. R. J. acknowledges the support by JSPS Overseas Challenge Program for Young Researchers 1080033.

DATA AVAILABILITY

The data that support the findings of this study are available from the corresponding author upon reasonable request.

REFERENCES

[1]V. G. Hill, R. Roy, and E. F. Osborn, J. Am. Chem. Soc. **35**, 135 (1952).
[2]H. Zhou, J. Zhang, C. Zhang, Q. Feng, S. Zhao, P. Ma, and Y. Hao, J. Semicon. **40**, 011803 (2019).
[3]M. Hilfiker, R. Korlacki, R. Jinno, Y. Cho, H. G. Xing, D. Jena, U. Kilic, M. Stokey, and M. Schubert, Appl. Phys. Lett. **118**, 062103 (2021).
[4]M. Higashiwaki and G. H. Jessen, Appl. Phys. Lett. **112**, 060401 (2018).
[5]M. Bosi, P. Mazzolini, L. Seravalli, and R. Fornari, J. Mater. Chem. C **8**, 10975 (2020).
[6]M. J. Tadjer, Electrochem. Soc. Int. **27**, 49 (2018).
[7]Y.-F. Wu, D. Kapolnek, J. Ibbetson, P. Parikh, B. Keller, and U. Mishra, IEEE Trans. Electron Devices **48**, 586 (2001).
[8]I. Akasaki, H. Amano, S. Sota, H. Sakai, T. Tanaka, and M. Koike, Jpn. J. Appl. Phys., Part 2 **34**, L1517 (1995).
[9]S. Nakamura, M. Senoh, S.-i. Nagahama, N. Iwasa, T. Yamada, T. Matsushita, H. Kiyoku, and Y. Sugimoto, Jpn. J. Appl. Phys., Part 2 **35**, L74 (1996).
[10]Q. Cai, H. You, H. Guo, J. Wang, B. Liu, Z. Xie, D. Chen, H. Lu, Y. Zheng, and R. Zhang, Light: Sci. Appl. **10**, 94 (2021).
[11]O. Ambacher, M. Arzberger, D. Brunner, H. Angerer, F. Freudenberg, N. Esser, T. Wethkamp, K. Wilmers, W. Richter, M. Stutzmann *et al.*, MRS Internet J. Nitride Semicond. Res. **2**, e22 (1997).
[12]G. Brummer, D. Nothern, A. Y. Nikiforov, and T. D. Moustakas, Appl. Phys. Lett. **106**, 221107 (2015).
[13]H. Peelaers, J. B. Varley, J. S. Speck, and C. G. Van de Walle, Appl. Phys. Lett. **112**, 242101 (2018).
[14]T. Wang, W. Li, C. Ni, and A. Janotti, Phys. Rev. Appl. **10**, 011003 (2018).
[15]A. Mock, R. Korlacki, C. Briley, V. Darakchieva, B. Monemar, Y. Kumagai, K. Goto, M. Higashiwaki, and M. Schubert, Phys. Rev. B **96**, 245205 (2017).
[16]C. Sturm, R. Schmidt-Grund, C. Kranert, J. Furthmüller, F. Bechstedt, and M. Grundmann, Phys. Rev. B **94**, 035148 (2016).
[17]C. Sturm, J. Furthmüller, F. Bechstedt, R. Schmidt-Grund, and M. Grundmann, APL Mater. **3**, 106106 (2015).
[18]Z. Galazka, Semicond. Sci. Technol. **33**, 113001 (2018).
[19]A. K. Harman, S. Ninomiya, and S. Adachi, J. Appl. Phys. **76**, 8032 (1994).
[20]R. H. Lyddane, R. G. Sachs, and E. Teller, Phys. Rev. **59**, 673 (1941).
[21]A. Mauze and J. Speck, "Plasma-assisted molecular beam epitaxy 1," in *Gallium Oxide: Materials Properties, Crystal Growth, and Devices*, edited by M. Higashiwaki and S. Fujita (Springer International Publishing, Cham, 2020), pp. 79–93.
[22]M. Hilfiker, U. Kilic, A. Mock, V. Darakchieva, S. Knight, R. Korlacki, A. Mauze, Y. Zhang, J. Speck, and M. Schubert, Appl. Phys. Lett. **114**, 231901 (2019).
[23]R. Jinno, C. S. Chang, T. Onuma, Y. Cho, S.-T. Ho, D. Rowe, M. C. Cao, K. Lee, V. Protasenko, D. G. Schlom, D. A. Muller, H. G. Xing, and D. Jena, Sci. Adv. **7**, eabd5891 (2021).
[24]D. S. Cook, J. E. Hooper, D. M. Dawson, J. M. Fisher, D. Thompsett, S. E. Ashbrook, and R. I. Walton, Inorg. Chem. **59**, 3805 (2020).
[25]H. Ito, K. Kaneko, and S. Fujita, Jpn. J. Appl. Phys., Part 1 **51**, 09LD16 (2012).
[26]S.-D. Lee, Y. Ito, K. Kaneko, and S. Fujita, Jpn. J. Appl. Phys., Part 1 **54**, 030301 (2015).
[27]T. Uchida, R. Jinno, S. Takemoto, K. Kaneko, and S. Fujita, Jpn. J. Appl. Phys., Part 1 **57**, 040314 (2018).
[28]G. T. Dang, T. Yasuoka, Y. Tagashira, T. Tadokoro, W. Theiss, and T. Kawaharamura, Appl. Phys. Lett. **113**, 062102 (2018).
[29]R. Jinno, K. Kaneko, and S. Fujita, Jpn. J. Appl. Phys., Part 1 **60**, SBBD13 (2021).
[30]Z. Chen, M. Arita, K. Saito, T. Tanaka, and Q. Guo, AIP Adv. **11**, 035319 (2021).
[31]R. Kumaran, T. Tiedje, S. E. Webster, S. Penson, and W. Li, Opt. Lett. **35**, 3793 (2010).
[32]M. Kracht, A. Karg, M. Feneberg, J. Bläsing, J. Schörmann, R. Goldhahn, and M. Eickhoff, Phys. Rev. Appl. **10**, 024047 (2018).
[33]M. Schubert, Ann. Phys. **15**, 480 (2006).
[34]M. Hilfiker, M. Stokey, R. Korlacki, U. Kilic, Z. Galazka, K. Irmscher, S. Zollner, and M. Schubert, Appl. Phys. Lett. **118**, 132102 (2021).
[35]M. Schubert, in *Handbook of Ellipsometry*, edited by E. Irene and H. Tompkins (William Andrew Publishing, 2004).
[36]P. Petrik, L. BirÁ, M. Fried, T. Lohner, R. Berger, C. Schneider, J. Gyulai, and H. Ryssel, Thin Solid Films **315**, 186 (1998).
[37]A. S. Barker, Phys. Rev. **132**, 1474 (1963).
[38]S. Pezzagna, J. Brault, M. Leroux, J. Massies, and M. de Micheli, J. Appl. Phys. **103**, 123112 (2008).